



## OPEN Magnetic susceptibility components reveal different aspects of neurodegeneration in alpha-synucleinopathies

Oliver C. Kiersnowski<sup>1</sup>, Pietro Mattioli<sup>1,2</sup>, Lucia Argenti<sup>2</sup>, Laura Avanzino<sup>1,3</sup>, Francesco Calizzano<sup>2</sup>, Andrea Diociasi<sup>1</sup>, Laura Falcitano<sup>1</sup>, Chunlei Liu<sup>4</sup>, Mattia Losa<sup>2</sup>, Federico Massa<sup>1,2</sup>, Silvia Morbelli<sup>5</sup>, Beatrice Orso<sup>2</sup>, Elisa Pelosin<sup>1,2</sup>, Stefano Raffa<sup>1</sup>, Matteo Pardini<sup>1,2</sup>, Dario Arnaldi<sup>1,2</sup>, Luca Roccatagliata<sup>1,6</sup>✉ & Mauro Costagli<sup>1,2</sup>

Nigrostriatal dopaminergic degeneration in alpha-synucleinopathies is indirectly reflected by low dopamine transporter (DaT) uptake through [123I]FP-CIT-SPECT. Bulk magnetic susceptibility ( $\chi$ ) in the substantia nigra, from MRI-based quantitative susceptibility mapping (QSM), is a potential biomarker of nigrostriatal degeneration, however, QSM cannot disentangle paramagnetic (e.g. iron) and diamagnetic (e.g. myelin) sources. Using the susceptibility source-separation technique DECOMPOSE, paramagnetic component susceptibility (PCS) and diamagnetic component susceptibility (DCS) were studied in prodromal and overt alpha-synucleinopathies, and their relationships with DaT-SPECT specific binding ratio (SBR) and clinical scores. 78 participants were included (23 controls, 30 prodromal and 25 overt alpha-synucleinopathies). Prodromal patients were subdivided into groups with positive or negative DaT-SPECT (SBR Z-scores below or above -1, respectively). Correlations of putamen and caudate SBR Z-scores with PCS and DCS in the substantia nigra, putamen, and caudate were investigated. Increased PCS was observed in the substantia nigra of prodromal alpha-synucleinopathy patients with positive DaT-SPECT compared to controls and prodromal patients with negative DaT-SPECT. SBR Z-scores in the putamen correlated with increased PCS in the substantia nigra and reduced |DCS| in the putamen, which may reflect dopaminergic degeneration ascribable to iron accumulation and nigrostriatal neuron axonal loss, respectively.

**Keywords** Alpha-synucleinopathies, Quantitative susceptibility mapping, DECOMPOSE, Susceptibility source separation, Parkinson's disease, Prodromal alpha-synucleinopathies

Parkinson's disease (PD) and dementia with Lewy bodies (DLB) are neurodegenerative diseases marked by abnormal alpha-synuclein (aSyn) accumulation in the brain<sup>1</sup>. Degeneration of dopaminergic neurons in the substantia nigra that project into the striatum<sup>2</sup> serves as a biomarker for neuronal aSyn diseases<sup>3</sup>, and reflects degeneration of the nigrostriatal dopaminergic pathway. This degeneration is usually assessed in clinical practice using molecular imaging techniques such as dopamine transporter (DaT) radioligand [123I]FP-CIT uptake through single photon emission computed tomography (SPECT)<sup>4</sup>. Alpha-synucleinopathies have a long prodromal stage before the emergence of overt neurological features such as parkinsonism and/or dementia. These prodromal stages include patients with idiopathic rapid eye movement behavior disorder (iRBD), and different subtypes of prodromal DLB (pDLB)<sup>5,6</sup>, such as pDLB with mild cognitive impairment (MCI-pDLB). Notably, nigrostriatal degeneration assessed by DaT-SPECT is among the strongest risk markers of short-term phenoconversion from prodromal to overt alpha-synucleinopathy stages, especially if a semi-quantitative<sup>7,8</sup> instead of a visual approach is applied<sup>5</sup>. In DaT-SPECT, the specific to non-displaceable binding ratio (SBR) is measured and compared to a healthy control distribution of SBR in the striatum using Z-scores<sup>9</sup>. Therefore, SBR

<sup>1</sup>IRCCS Ospedale Policlinico San Martino, Genova, Italy. <sup>2</sup>Department of Neuroscience, Rehabilitation, Ophthalmology, Genetics, Maternal and Child Health, University of Genova, Genova, Italy. <sup>3</sup>Department of Experimental Medicine, University of Genova, Genova, Italy. <sup>4</sup>University of California Berkeley, Berkeley, United States of America. <sup>5</sup>Department of Nuclear Medicine, University of Turin, Turin, Italy. <sup>6</sup>Department of Health Sciences, University of Genova, Genova, Italy. ✉email: lroccatagliata@neurologia.unige.it

Z-score analysis aids in both the diagnosis of overt aSyn and assessing the risk of phenoconversion of prodromal aSyn.

Two biological definitions based on the presence of pathological alpha-synuclein aggregates, a hallmark of both PD and DLB, irrespective of clinical presentations, have recently been proposed<sup>3,10</sup>. Both highlight the role of molecular imaging with fluorodopa or with tracers for the dopamine transporter (DaT-SPECT) to detect dopaminergic degeneration and neurodegeneration<sup>3,10</sup>, while only one<sup>10</sup> suggests the use of MRI advanced techniques for evaluating substantia nigra neurodegeneration as an investigational biomarker. As the relative availability of molecular imaging techniques may be heterogenous among centers and considering the common use of MRI as a gateway exam in subjects with suspected neurodegenerative diseases, recent years have seen increased interest in MRI-based approaches to study the extent of in vivo nigrostriatal degeneration<sup>11–15</sup>.

Quantitative susceptibility mapping (QSM) is a magnetic resonance imaging (MRI) technique that reconstructs spatial maps of magnetic susceptibility ( $\chi$ ) from the raw phase component of the MRI signal<sup>16–20</sup>. QSM has identified changes in  $\chi$  in the substantia nigra between healthy controls and degenerative Parkinsonisms, such as PD<sup>21–24</sup>, attributable to an increase in the concentration of paramagnetic iron in the form of ferritin in the substantia nigra. Recently, QSM has also identified increases in  $\chi$  in the substantia nigra in iRBD patients compared to healthy controls, alongside the expected  $\chi$  increases in PD patients<sup>12,13</sup>, indicating that the accumulation of iron may occur years prior to the appearance of overt clinical symptoms. Other work has identified significant correlations between DaT-SPECT SBR scores and  $\chi$  in the substantia nigra of PD patients<sup>14,25</sup> and iRBD patients<sup>13,25</sup>. Visual assessment using susceptibility weighted imaging (SWI) also found that iRBD patients can display a loss of dorsal nigral hyperintensity correlated with greater dopaminergic degeneration<sup>11,12,15</sup>.

QSM, alongside transverse relaxation rate ( $R2^*$ ) mapping, provides insights into the pathological causes behind these identified  $\chi$  changes, such as increased iron and/or decreased myelin content. However, QSM provides bulk tissue  $\chi$  estimates, whereby all susceptibility sources within a voxel are averaged providing a single value. Therefore, any subtle pathological changes that specifically affect paramagnetic ( $\chi^+$ ) or diamagnetic ( $\chi^-$ ) sources are difficult to distinguish. The novel  $\chi$  source separation technique, DECOMPOSE<sup>26</sup>, disentangles the signal from  $\chi^+$  and  $\chi^-$  sources by calculating the paramagnetic component susceptibility (PCS) and the diamagnetic component susceptibility (DCS) allowing for a more nuanced investigation; for example, changes in PCS may be attributable to iron whereas DCS changes are more attributable to myelin changes and/or calcium deposition. DECOMPOSE has had success in identifying whole-brain DCS changes in Alzheimer's disease (AD)<sup>27</sup> and its value in clinical research is growing<sup>28</sup>. It is important to note that DECOMPOSE may not always result in a larger effect size compared to QSM when measuring susceptibility-based changes. For instance, in cases where both iron deposition and demyelination occur simultaneously in the same region, QSM would likely show a greater overall effect size because it captures the combined impact of both factors. In contrast, DECOMPOSE separates these effects, potentially yielding smaller but more specific measurements for each individual component.

We set out to investigate changes in  $\chi$ , PCS and DCS using standard QSM and DECOMPOSE, across patients along the prodromal to overt alpha-synucleinopathy continuum, compared to control subjects, attempting to further understand the specific mechanisms of tissue composition changes in the substantia nigra and striatum. We also investigated correlations between DaT-SPECT SBR Z-scores with  $\chi$ , PCS and DCS in the substantia nigra and in the putamen and caudate, with the aim of supporting  $\chi$  as a possible biomarker for assessing substantia nigra neurodegeneration and introducing PCS and DCS as additional biomarkers with complimentary and novel information.

## Methods

### Participants

A total of 87 consecutive participants were recruited for this study, including 26 healthy controls (HCs), 34 prodromal aSyn and 27 overt aSyn, who attended the Memory Clinic of the IRCCS Ospedale Policlinico San Martino, Genova, Italy due to cognitive, motor or sleep complaints. All participants underwent MRI acquisition and prodromal aSyn patients also underwent DaT-SPECT.

Visual quality control of MRI images resulted in the removal of 9 patients (3 HC, 4 prodromal and 2 overt aSyn) from further analysis due to the presence of artifacts, such as gross subject motion. Therefore, a total of 78 participants underwent analysis (23 HC, 30 prodromal and 25 overt aSyn). See Table 1 for demographic information with specific diagnoses in the prodromal and overt aSyn groups.

For all prodromal and overt aSyn participants, scores from the Movement Disorder Society-Sponsored Revision of the Unified Parkinson's Disease Rating Scale, Part III (MDS-UPDRS III) were recorded. Cognitive assessments were available for all prodromal aSyn and DLB patients through the Mini-Mental State Examination (MMSE), while PD patients in the overt aSyn group had Montreal Cognitive Assessment (MoCA) scores, which were subsequently converted to MMSE scores<sup>29</sup>. At the time of examination, neither the prodromal aSyn nor DLB patients were undergoing medical treatment. However, PD patients were receiving medical intervention (Levodopa equivalent daily dose [LEDD] mean dose 620.30 mg, SD 161.49 mg; see Table 1).

### Diagnostic protocol

Diagnoses were made based on the following criteria: MDS clinical diagnostic criteria for PD<sup>30</sup>, International Classification of Sleep Disorders – Third Edition (ICSD-3) criteria for iRBD<sup>31</sup>, revised criteria from the DLB Consortium for DLB<sup>32</sup> and research criteria for pDLB<sup>6</sup>. We defined as prodromal alpha-synucleinopathy patients those that satisfied either iRBD or pDLB criteria. A healthy control cohort comprised age-matched individuals with no history of neurological or psychiatric disorders. These volunteers were recruited from among family members and acquaintances of patients and hospital staff.

	Healthy Controls n = 23	Prodromal Negative aSyn n = 11	Prodromal Positive aSyn n = 19	Overt aSyn n = 25	P value (post-hoc values in parentheses)
Diagnosis <i>Diagnosis: n</i>	n/a	iRBD: 9 pDLB: 2	iRBD: 10 pDLB: 9	PD: 21 DLB: 4	
Age Range; median (IQR) (years)	55.0; 73.0 (13.0)	23.0; 72.0 (10.0)	31.0; 74.0 (9.5)	30.0; 71.0 (7.0)	0.225
Sex Female/Male ( <i>n</i> )	17/6	3/8	7/12	10/15	0.022 (post-hoc tests n.s.)
Disease Duration mean; SD (years)	n/a	1.96; 2.89	0.94; 1.34	7.00; 4.36	0.312*
Hoehn and Yahr Stage mean; SD	n/a	0.91; 0.51	1.26; 0.64	1.63; 0.52	0.005 (0.002 <sup>a</sup> )
MDS-UPDRS III mean; SD	n/a	3.27; 2.86	8.21; 7.80	19.84; 10.47	<0.001 (<0.001 <sup>a,b</sup> )
MMSE mean; SD	n/a	27.82; 2.37	27.26; 3.39	26.14; 5.00	0.948
LEDD <sup>†</sup> mean; SD (mg)	n/a	n/a	n/a	620.30; 161.49	

**Table 1.** Demographic information of patients who underwent analysis. The prodromal aSyn group comprised iRBD and pDLB patients with mild cognitive impairment (MCI-pDLB), and overt aSyn comprised PD and DLB patients. Prodromal aSyn patients underwent a DAT-SPECT scan to assess the function of the dopaminergic pathway, leading to a splitting of the prodromal group based on positive/negative DAT-SPECT defined as SBR of the most affected putamen being less than or greater than -1, respectively. Disease duration is defined as the time between diagnosis and MRI examination for this study. P-value column provides the p-value from group-wise statistical tests comparing demographics; significant p values from post-hoc statistical tests are provided in parentheses. Post-hoc p value comparisons: *a*: comparison between prodromal negative aSyn and overt aSyn. *b*: comparison between prodromal positive aSyn and overt aSyn. aSyn: alpha-synucleinopathy; iRBD: idiopathic REM Behavioral Disorder; pDLB: prodromal dementia with Lewy bodies; PD: Parkinson's disease; DLB: Dementia with Lewy bodies; IQR: interquartile range; SD: standard deviation; n.s.: not significant; MDS-UPDRS III: Movement Disorder Society-Sponsored Revision of the Unified Parkinson's Disease Rating Scale, Part III; MMSE: mini-mental state examination; LEDD: Levodopa equivalent daily dose [\*] \* comparison of disease duration between prodromal aSyn patients with negative and positive DaT-SPECT [\*] † PD patients alone; within the overt aSyn group, PD patients were undergoing medical intervention whereas DLB patients were not, therefore, the LEDD values presented here are from the PD patients alone

## Data acquisition and processing

### MRI acquisition

Whole-brain magnitude and raw phase data were acquired for all participants on a Siemens Prisma 3T MRI system (IRCCS Ospedale Policlinico San Martino, Genova, Italy) using a multi-echo 3D gradient echo (GRE) sequence optimised for QSM<sup>33</sup> with eight echoes at TE1/TE/TE<sub>max</sub> = 5.6/5.6/44.8 ms; TR = 51 ms; flip angle 18°; 1 × 1 × 1 mm<sup>3</sup> resolution; 224 × 224 × 144 matrix size; GRAPPA = 2; partial Fourier 6/8 in both PE directions; BW = 340 Hz/px; adaptive coil combine with pre-scan normalize on; acquisition time = 8 min 45 s; pure-axial acquisition<sup>34</sup>.

Structural brain images were also acquired in the sagittal plane via a T1-weighted MPRAGE with TR = 2300 ms; TE = 2.96 ms; TI = 900 ms; flip angle 9°; 1 × 1 × 1 mm<sup>3</sup> resolution; 256 × 256 matrix size; GRAPPA = 2; BW = 240 Hz/px; acquisition time = 5 min 30 s. T1-weighted images were rigidly registered to the combined GRE magnitude images for each patient via FSL FLIRT<sup>35,36</sup>.

### MRI processing

For each participant, an R2\* map, susceptibility map, and PCS and DCS maps were reconstructed (Figure 1). All image reconstructions were carried out using Matlab 2019b (MathWorks, USA), as follows.

R2\* maps were calculated via the Auto-Regression of Linear Operations (ARLO) method<sup>37</sup> from the MEDI Toolbox<sup>38</sup>.

Susceptibility maps were reconstructed in accordance with the International Society for Magnetic Resonance Imaging (ISMRM) Electromagnetic Tissue Study Group's (EMTP) recommendations<sup>39</sup> using STI Suite (<https://people.eecs.berkeley.edu/~chunlei.liu/software.html> from UC Berkeley, Berkeley, CA, USA). A brain mask was calculated from the T2\*-weighted magnitude image averaged across all echoes using the Brain Extraction Tool (BET) from FSL<sup>40</sup>. A total field map was obtained from a non-linear fit of the complex data over all echoes<sup>41</sup>, and residual phase wraps were unwrapped using Laplacian phase unwrapping<sup>42</sup> followed by background field removal using the variable-kernel sophisticated harmonic artifact reduction for phase data (V-SHARP) approach<sup>43</sup>. Tissue bulk susceptibility,  $\chi$ , maps were then calculated using the iLSQR method<sup>44</sup>.

Maps of PCS and DCS were calculated using DECOMPOSE<sup>26</sup> whereby a QSM calculated at each echo were used to create a 3-pool signal model of paramagnetic, diamagnetic and magnetically neutral material. Only the first five echoes were used in DECOMPOSE reconstructions as later echoes often suffered from a low signal-to-noise ratio and phase artefacts, which were more easily dealt with by the non-linear fitting in the QSM processing.

The caudate, putamen and substantia nigra were segmented automatically using MRI Cloud<sup>45,46</sup> and eroded by a 1 mm spherical kernel to avoid partial volume effects.

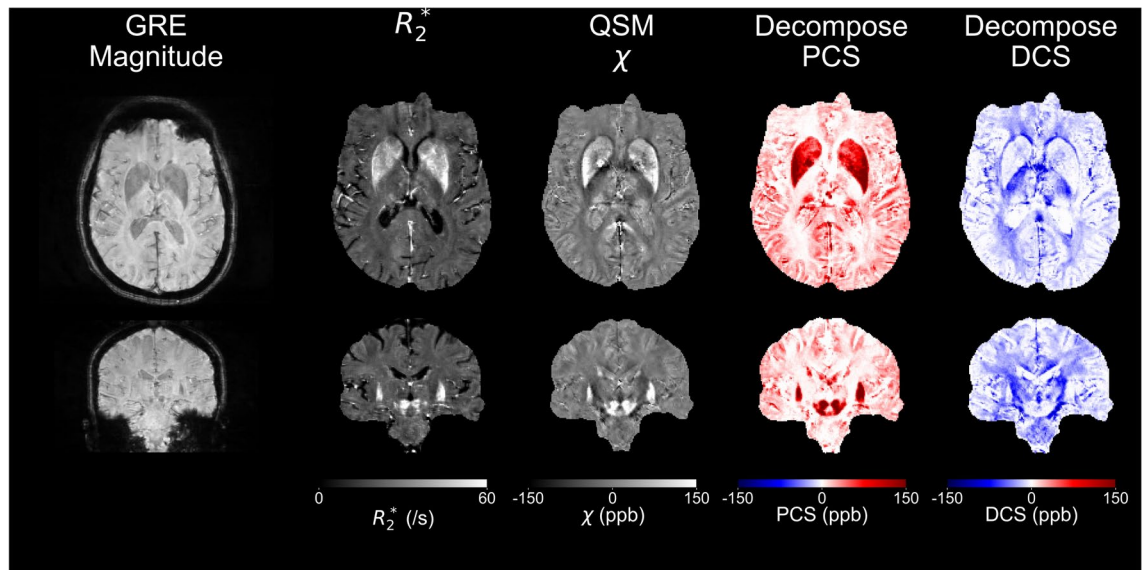


**Fig. 1.** Axial and coronal views (from left to right) of combined MRI gradient echo (GRE) magnitude,  $R_2^*$ , QSM, and DECOMPOSE paramagnetic and diamagnetic component susceptibility (PCS and DCS, respectively) maps in an example healthy control participant.

#### *[<sup>123</sup>I]-Ioflupane SPECT*

Assessment of nigrostriatal dopaminergic function in the prodromal aSyn group was carried out by a clinically routine <sup>123</sup>I-*ioflupane* contrast injection (DaTSCAN, GE Healthcare) according to established guidelines<sup>47</sup> on a two-headed GE Millennium VG camera. Semi-quantification of DaT-SPECT images was carried out by DaTQUANT™ software (GE Healthcare) with bilateral partial volume corrected SBR values at the putamen and caudate levels, using occipital lobe tracer uptake values as reference. Age and sex-corrected Z-scores were then calculated with reference to an established healthy control cohort as previously described<sup>8</sup>.

Prodromal aSyn patients were then subdivided into two groups based on the presence of a DaT-SPECT Z-score below -1 (prodromal positive) or above -1 (prodromal negative) in the most affected putamen<sup>8,9</sup>, with 11 patients being named prodromal negative and 19 prodromal positive (Table 1). This cut-off was chosen based on recent studies investigating the most sensitive cut-off for the identification of iRBD patients that later converted to PD/DLB as well as for prodromal and overt DLB<sup>8,9,48,49</sup>.

#### Statistical analysis

Variables were tested for normality using the Shapiro-Wilk's test with a significance threshold of  $p < 0.01$ . Bulk  $\chi$ , PCS, DCS and  $R_2^*$  values in all ROIs were corrected for age by residualisation based on a linear fit<sup>50–52</sup> of susceptibility/ $R_2^*$  against age in the HC group.

Demographics and clinical characteristics were compared across all groups (HC, prodromal negative, prodromal positive and overt aSyn) and across only patient groups (prodromal negative, prodromal positive and overt aSyn) when appropriate with significant level  $p = 0.05$ . Differences in age, Hoehn & Yahr stages, MDS-UPDRS III and MMSE were assessed using non-parametric Kruskal-Wallis H-tests with post-hoc t-tests. Differences in sex were assessed using a chi-squared test followed by post-hoc chi-squared tests comparing each group individually. All post-hoc statistical tests were FDR-corrected for multiple comparisons.

Four group two-tailed analysis of covariance (ANCOVA) was then performed in the substantia nigra from both hemispheres to investigate differences between age-corrected  $\chi$ , PCS, DCS and  $R_2^*$  across disease groups with sex included as a confounding factor. Here,  $\eta^2$  was used as a measure of the effect size. Post-hoc Welch's t-tests were carried out to identify which groups were significantly different to one another, with FDR-corrected  $q < 0.05$  indicating statistical significance and Cohen's  $d$  representing the effect size for the t-tests.

Within the prodromal alpha-synucleinopathy group,  $\chi$ , PCS and DCS in the putamen, caudate and substantia nigra were correlated to DaT-SPECT SBR Z-scores at the putamen and caudate level using linear regressions with p-values FDR-corrected for multiple comparisons.

Finally, SBR Z-scores and DCS in the most affected putamen, alongside  $\chi$  and PCS in the substantia nigra corresponding to the side of the most affected putamen, were correlated against clinical MDS-UPDRS III and MMSE scores. If the residuals of the correlation were non-normal, the correlation was made against the  $\log(\text{MDS-UPDRS III} + 1)$  or  $\log(\text{MMSE})$ .

All statistical analysis was performed using Python 3.11.7 with the Scipy package.

#### Ethics declaration

This study was ethically approved by the regional ethics board “Comitato Etico Regionale (CER) Liguria” (N. Registro CER Liguria: 168/2022 – DB id 12248) and was, therefore, performed in accordance with the ethical

standards laid down in the 1964 Declaration of Helsinki and its later amendments. All enrolled patients and healthy volunteers provided their informed consent.

## Results

### Demographics and clinical characteristics

Ages across cohorts were non-normal and not significantly different ( $p = 0.225$ ) while ratio of male/female was significantly different ( $p = 0.022$ ) across the four groups. No individual group differences from post-hoc tests comparing the ratio of male/female survived FDR correction. There were no significant differences in disease duration between prodromal patients with negative and positive DaT-SPECT ( $p = 0.312$ ). A non-parametric Kruskal-Wallis test revealed significant differences in Hoehn and Yahr stages between disease groups ( $p = 0.005$ ), with post-hoc tests showing that the overt aSyn group had a significantly higher Hoehn and Yahr stage than the prodromal negative group ( $p = 0.002$ ). Hoehn and Yahr stages were not significantly different between prodromal negative and positive groups or between prodromal positive aSyn and overt aSyn groups. Kruskal-Wallis groupwise comparison showed significant differences in MDS-UPDRS III across the three disease groups ( $p < 0.001$ ), with post-hoc tests showing significantly higher MDS-UPDRS III in the overt group compared to both prodromal negative and prodromal positive aSyn groups ( $p < 0.001$  for both). No significant differences were observed between prodromal negative and prodromal positive aSyn groups. No differences in MMSE between the disease groups were found ( $p = 0.948$ ).

### Substantia nigra susceptibility differences across groups

As seen in Figure 2, the distributions of  $\chi$ , PCS, DCS and  $R2^*$  were not significantly different from the normal distribution. One-way ANCOVA revealed significant differences in mean and PCS in the substantia nigra between groups ( $q < 0.001$  for both). Sex was not found to be a significant covariate for  $\chi$ , PCS, DCS or  $R2^*$ .

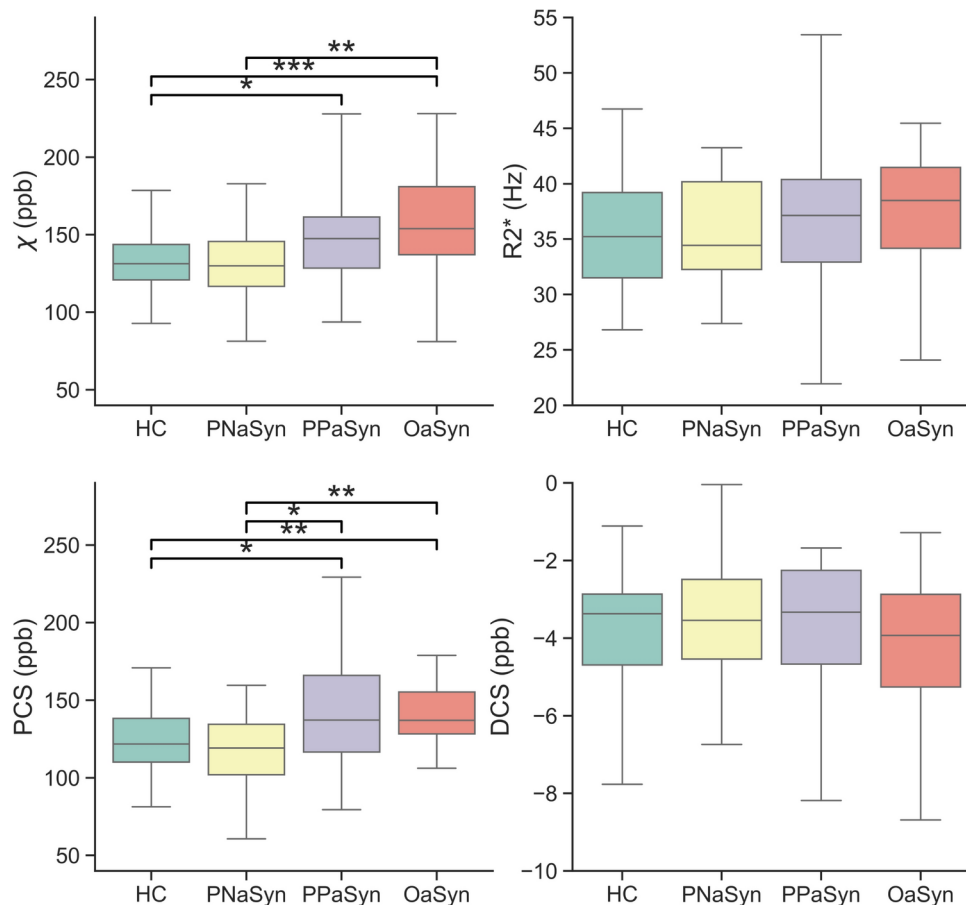


**Fig. 2.** Mean  $\chi$ , PCS, DCS and  $R2^*$  in the substantia nigra across groups. One-way ANCOVA revealed significant differences in  $\chi$  and PCS between groups, with post-hoc t-tests indicating significantly higher substantia nigra  $\chi$  and PCS in overt aSyn and prodromal positive aSyn patients compared to both HCs and prodromal negative aSyn patients. Overt aSyn patients also exhibit higher  $\chi$  and PCS in the substantia nigra than prodromal negative aSyn patients. However, a difference between prodromal positive aSyn and prodromal negative aSyn patients was only observable in the PCS. \* indicates  $q < 0.05$ , \*\* indicates  $q < 0.01$  and \*\*\*  $q < 0.001$ ; HC: healthy controls; PNaSyn: prodromal negative alpha-synucleinopathies; PPaSyn prodromal positive alpha-synucleinopathies; OaSyn: overt alpha-synucleinopathies; ppb: parts per billion.

	Susceptibility ( $\chi$ )	Paramagnetic Component Susceptibility (PCS)	Diamagnetic Component Susceptibility (DCS)	Transverse Relaxation Rate ( $R2^*$ )
<b>ANCOVA</b>				
$q$	< <b>0.001</b>	< <b>0.001</b>	0.274	0.252
$\eta^2$	0.151	0.122	0.025	0.032
Post-hoc t tests $q$ -value (Cohen's $d$ )				
HC v PNaSyn	0.902 (0.039)	0.392 (0.277)	0.987 (-0.016)	0.928 (-0.033)
HC v PPaSyn	<b>0.039 (-0.582)</b>	<b>0.033 (-0.538)</b>	0.987 (-0.022)	0.265 (-0.375)
HC v OaSyn	< <b>0.001 (-1.032)</b>	<b>0.002 (-0.793)</b>	0.426 (0.321)	0.265 (-0.412)
PNaSyn v PPaSyn	0.104 (-0.515)	<b>0.017 (-0.677)</b>	0.987 (-0.005)	0.290 (-0.328)
PNaSyn v OaSyn	<b>0.005 (-0.920)</b>	<b>0.003 (-1.056)</b>	0.435 (0.300)	0.265 (-0.378)
PPaSyn v OaSyn	0.150 (-0.355)	0.876 (-0.036)	0.426 (0.315)	0.928 (0.021)

**Table 2.** Results for one-way ANCOVA for groupwise comparisons of mean  $\chi$ , PCS, DCS and  $R2^*$ . ANCOVA with post-hoc Welch's t-tests were carried out with Cohen's  $d$  reflecting the effect size. FDR-corrected  $q$ -values are shown for both group-wise tests and post-hoc tests. Bold entries indicate significance at the  $q < 0.05$  level HC: healthy controls; PNaSyn: prodromal negative alpha-synucleinopathies; PPaSyn: prodromal positive alpha-synucleinopathies; OaSyn: overt alpha-synucleinopathies; ANCOVA: analysis of covariance

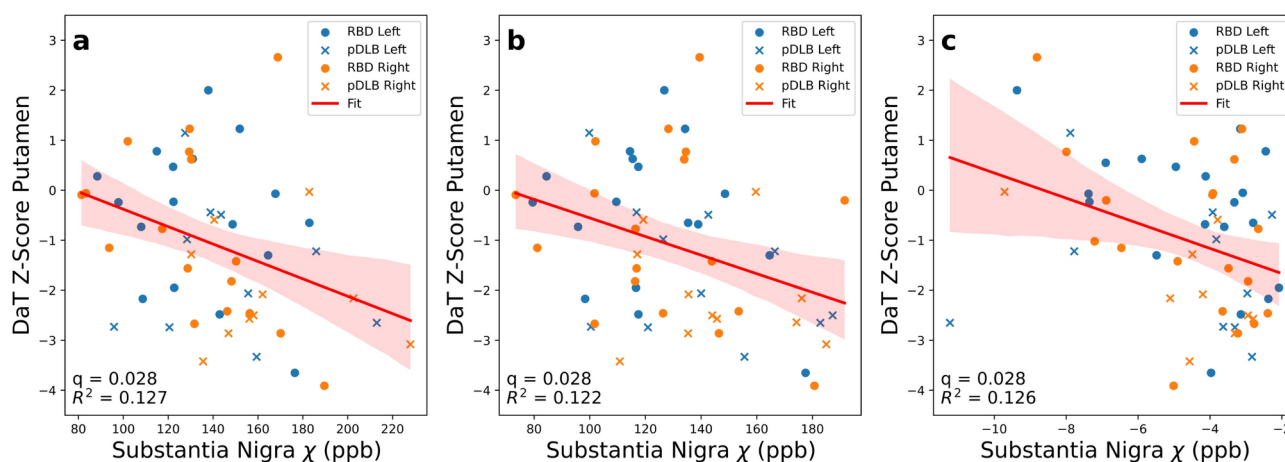


**Fig. 3.** Significant negative linear correlations in the prodromal alpha-synucleinopathy group were identified between DaT-SPECT SBR Z-scores in the putamen and  $\chi$  in the substantia nigra (A), PCS in the substantia nigra (B) and DCS in the putamen (C). Panels A and B indicate that greater dopaminergic degeneration at the putamen level, reflected by a lower SBR Z-score from DaT-SPECT, is associated with an increase in concentration of paramagnetic sources (greater  $\chi$  and PCS), attributable to iron accumulation. Panel C shows that greater dopaminergic degeneration at the putamen level is also correlated with a decrease in the concentration of diamagnetic sources in the putamen.

. Post-hoc t-tests revealed significantly higher substantia nigra  $\chi$  in the overt aSyn group compared to HC and prodromal negative aSyn ( $q < 0.001$  and  $q = 0.005$ , respectively), which were complemented by the same findings in PCS ( $q = 0.002$  and  $q = 0.003$  between HC and prodromal negative aSyn subjects, respectively). The prodromal positive aSyn group had a significantly higher  $\chi$  and PCS in the substantia nigra compared to the HCs as well ( $q = 0.039$  and  $q = 0.033$ ). The prodromal positive aSyn group also had a significantly higher PCS compared to the prodromal negative aSyn group, but not in  $\chi$ . There were no significant differences in substantia nigra mean  $R2^*$  or DCS according to ANCOVA tests ( $q = 0.252$  and  $0.274$ , respectively), although for  $R2^*$  an uncorrected t-test between HC and overt aSyn of  $p = 0.049$  suggest an expected trend of increased  $R2^*$  in overt aSyn patients compared to HCs, in line with susceptibility findings. Specific details and effect sizes can be found in Table 2.

### Correlations of DaT-SPECT, susceptibility and clinical scores

DaT-SPECT SBR Z-scores at the putamen level were significantly negatively correlated with  $\chi$  and PCS measured in the substantia nigra ( $q = 0.028$  for both; Figure 3A and 3B). Significant negative correlations were also identified between DaT-SPECT SBR Z-scores and DCS at the putamen level ( $q = 0.028$ ; Figure 3C). The same correlations of SBR Z-scores at the putamen level and standard QSM  $\chi$  in the putamen were not identified ( $q = 0.378$ ).

After FDR correction, no significant correlations were identified between clinical MDS-UPDRS III or MMSE scores and DaT-SPECT SBR Z-scores and DCS in the most affected putamen, nor with  $\chi$  and PCS in the substantia nigra (Figure 4).

A summary of all correlations investigated can be found in Table 3.

## Discussion

In this study, we applied QSM and the novel susceptibility source-separation method DECOMPOSE<sup>26</sup> to investigate changes in  $\chi$ , and its para/diamagnetic components (PCS and DCS), alongside  $R_2^*$  in the substantia nigra across patients with prodromal and overt stages of alpha-synuclein disease compared to healthy controls. We identified a clear increase of bulk susceptibility ( $\chi$ ) in overt alpha-synucleinopathy patients compared to both HCs and prodromal patients with a negative DaT-SPECT. For the first time, we found increased mean PCS in the substantia nigra of prodromal patients with positive DaT-SPECT compared to HCs and prodromal patients with a negative DaT-SPECT. Finally, we identified significant correlations between the DaT-SPECT SBR Z-scores at the putamen level, a biomarker of nigrostriatal dopaminergic function, and  $\chi$  and PCS in the substantia nigra and DCS in the putamen. These results suggest that susceptibility imaging may be a candidate metric to evaluate substantia nigra neurodegeneration in alpha-synucleinopathies, providing complimentary and/or overlapping information to DaT-SPECT in the future.

Magnetic susceptibility in tissue is a correlate for paramagnetic sources (e.g. iron) and diamagnetic sources (e.g. myelin)<sup>19,53</sup>. Ferrous iron can induce cell loss and aSyn aggregation in the substantia nigra<sup>14,54</sup>, making susceptibility a correlate of interest for aSyn disease. An increase in bulk magnetic susceptibility,  $\chi$ , calculated from QSM, can be attributable to an increased concentration of paramagnetic sources or a decreased concentration of diamagnetic sources. To understand this,  $\chi$  is often used alongside  $R_2^*$  as it is a measure of the concentration of susceptibility sources irrespective of their para/diamagnetism. An increase in  $\chi$  alongside an increase in  $R_2^*$  indicates an increased concentration of paramagnetic susceptibility sources, whereas an increase in  $\chi$  alongside a decrease in  $R_2^*$  is attributable to a reduced concentration of diamagnetic sources. However,  $\chi$  and  $R_2^*$  are estimates of the mean bulk susceptibility, averaging both paramagnetic and diamagnetic material<sup>19</sup>, making it difficult to separate pathological changes that affect both types of sources simultaneously. Susceptibility source separation methods<sup>26,55,56</sup> provide a more detailed and specific view of changes in tissue composition.

While a significant difference in sex was identified between groups ( $p = 0.022$ , Table 1), our ANCOVA analysis revealed that sex was not a significant covariate of  $\chi$ , PCS, DCS or  $R_2^*$ . This agrees with the vast majority of literature that has not identified any sex-dependence on measured susceptibility<sup>57</sup>. Therefore, susceptibility-based findings across groups in this study are not affected by the differences in sex of the cohorts.

In patients in overt stages of alpha-synucleinopathies and prodromal stages with positive DaT-SPECT, an increase in mean bulk  $\chi$  in the substantia nigra was observed compared to HCs and prodromal negative aSyn patients using standard QSM, consistent with literature<sup>13,15,21–24,58–60</sup> (Figure 2). DECOMPOSE, however, showed increased PCS in prodromal alpha-synucleinopathy patients with positive DaT-SPECT compared to those with negative DaT-SPECT in the substantia nigra, not evident in  $\chi$  changes. This significant PCS increase in prodromal aSyn patients with positive DaT-SPECT suggests that DECOMPOSE-QSM can identify more

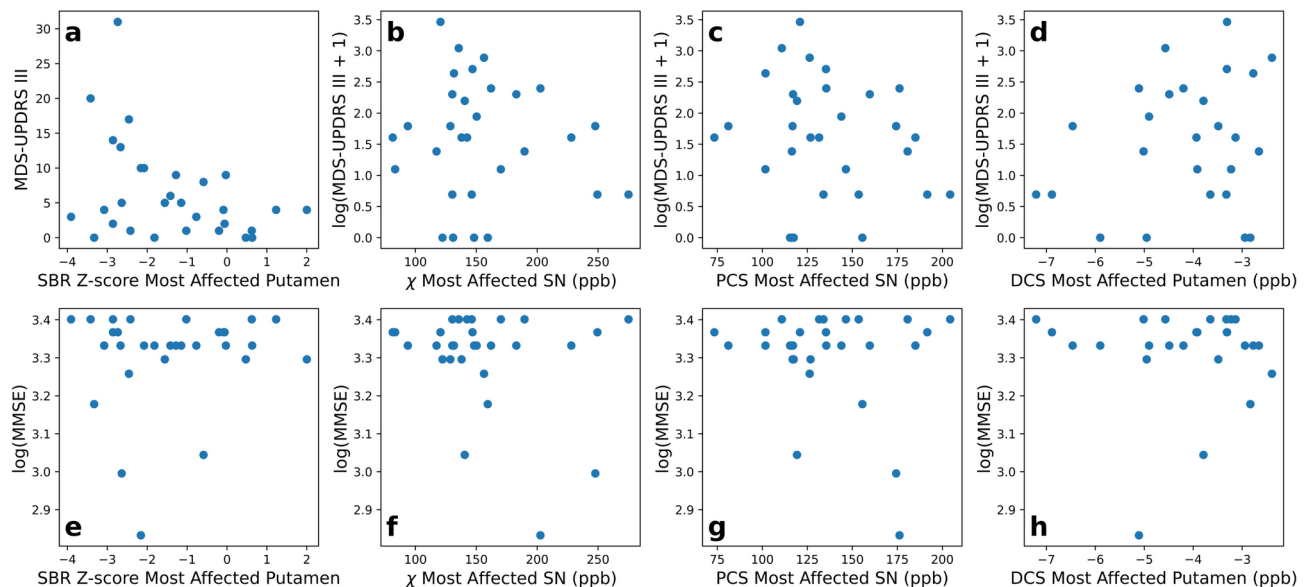


**Fig. 4.** Clinical MDS-UPDRS III scores in the most affected putamen (top row) and mini-mental state examination (MMSE) scores (bottom row) in the prodromal alpha-synucleinopathy group against (a, e) DaT-SPECT Z-scores in the most affected putamen, (b, f) bulk susceptibility in the most affected substantia nigra, (c, g) PCS in the most affected substantia nigra, and (d, h) DCS in the most affected putamen. No significant correlations were identified post-FDR correction.

Comparison	Linear Regression Coefficient coefficient (confidence interval)	Coefficient of Determination ( $R^2$ )	Uncorrected p-value	FDR Corrected q-value
<b>DaT-SPECT Putamen</b>				
- vs $\chi$ substantia nigra	<b>-0.017 (-0.030 to -0.005)</b>	<b>0.127</b>	0.004	<b>0.028</b>
- vs PCS substantia nigra	<b>-0.019 (-0.032 to 0.005)</b>	<b>0.122</b>	0.004	<b>0.028</b>
- vs DCS substantia nigra	-0.233 (-0.482 to 0.016)	0.061	0.066	0.147
- vs $\chi$ putamen	0.014 (-0.013 to 0.042)	0.020	0.299	0.378
- vs PCS putamen	-0.001 (-0.023 to 0.021)	0.000	0.937	0.937
- vs DCS putamen	<b>-0.251 (-0.430 to -0.072)</b>	<b>0.126</b>	0.003	<b>0.028</b>
<b>DaT-SPECT Caudate</b>				
- vs $\chi$ substantia nigra	-0.001 (-0.019 to 0.002)	0.050	0.052	0.129
- vs PCS substantia nigra	-0.010 (-0.021 to 0.000)	0.063	0.030	0.093
- vs DCS substantia nigra	-0.058 (-0.261 to 0.145)	0.006	0.571	0.601
- vs $\chi$ caudate	0.029 (0.006 to 0.051)	.104	0.104	0.069
- vs PCS caudate	0.0232 (0.002 to 0.045)	0.079	0.033	0.093
- vs DCS caudate	-0.046 (-0.265 to 0.175)	0.003	0.339	0.399
<b>MDS-UPDRS III</b>				
- vs DaT-SPECT most affected putamen	-1.770 (-3.402 to -0.139)	0.150	0.017	0.069
- vs $\chi$ most affected substantia nigra	-0.002 (-0.010 to 0.006)	0.010	0.303	0.378
- vs PCS most affected substantia nigra	-0.005 (-0.016 to 0.006)	0.029	0.186	0.286
- vs DCS most affected putamen	0.173 (-0.143 to 0.489)	0.050	0.135	0.246
<b>MMSE</b>				
- vs DaT-SPECT most affected putamen	0.010 (-0.023 to 0.043)	0.013	0.274	0.378
- vs $\chi$ most affected substantia nigra	-0.001 (-0.002 to 0.000)	0.064	0.089	0.177
- vs PCS most affected substantia nigra	-0.001 (-0.002 to 0.001)	0.038	0.152	0.254
- vs DCS most affected putamen	-0.001 (-0.041 to 0.039)	0.000	0.473	0.526

**Table 3.** Summary of statistical results of linear regressions investigating correlations between DaT-SPECT in the putamen and caudate with susceptibility, PCS and DCS in the substantia nigra, putamen and caudate. Clinical comparisons of MDS-UPDRS III and MMSE clinical scores with DaT-SPECT and DCS in the most affected putamen, and  $\chi$  and PCS in the most affected substantia nigra are also shown. DaT-SPECT: dopamine transporter single photon emission computed tomography; PCS: paramagnetic component susceptibility; DCS: diamagnetic component susceptibility; MDS-UPDRS III: Movement Disorder Society-Sponsored Revision of the Unified Parkinson's Disease Rating Scale, Part III; MMSE: Mini-mental state examination

subtle, early susceptibility alteration, prior to the onset of overt motor symptoms as reflected by the low average prodromal MDS-UPDRS III score of 6.40 showing minimal motor symptoms in the prodromal cohort. No significant differences in PCS in the substantia nigra of prodromal positive and overt aSyn patients indicate iron accumulation in the substantia nigra occurs in the prodromal stages with a plateau effect. This is further supported by the lack of differences between HC and prodromal negative aSyn groups. This aligns with recent literature<sup>12,61</sup> showing early iron accumulation in PD with no stage-wise differences within PD patients, i.e. Hoehn & Yahr stage I vs IV. The lack of group differences in mean DCS in the substantia nigra suggests iron accumulation, rather than myelin reduction that may be observed once neuronal loss has occurred<sup>62</sup>, drives deterioration. Large standard deviations DCS boxplots (Figure 2) may have contributed to this lack of findings, therefore, further investigation with larger sample sizes is needed. Overall,  $\chi$  and PCS may be useful non-invasive MRI metrics for evaluating substantia nigra neurodegeneration in alpha-synucleinopathies, even in prodromal stages.

DaT-SPECT imaging is widely used to assess nigrostriatal dopaminergic integrity in neurodegenerative parkinsonism<sup>63</sup> and can be used in the prediction of phenoconversion from prodromal to overt alpha-synucleinopathy stages, especially when used in conjunction with clinical features<sup>7,8</sup>. However, DaT-SPECT is of limited availability and requires the injection of a radiopharmaceutical labelled with  $\gamma$ -ray emitting <sup>123</sup>I. In this study, DaT-SPECT SBR Z-scores at the putamen level were significantly negatively correlated with  $\chi$  and PCS in the substantia nigra in prodromal aSyn patients (Figure 3). The deterioration of the dopaminergic pathway assessed by DaT-SPECT is associated with nigrostriatal neuron deterioration in the substantia nigra projecting into the striatum. It is not, therefore, surprising that greater dopaminergic degeneration as reflected by a lower SBR Z-score from DaT-SPECT, is correlated with a higher mean  $\chi$  and PCS in the substantia nigra, attributable to iron accumulation, and thus neuronal loss<sup>54,64</sup>. This correlation between DaT-SPECT and  $\chi$  in prodromal alpha-synucleinopathies aligns with literature showing significant correlations between posterior putamen DaT-SPECT uptake and in the substantia nigra pars reticularis, compacta and nigrosome 1 (N1) in iRBD patients<sup>13</sup>. Proper segmentation of substantia nigra substructures like N1 is challenging, especially at the electromagnetic tissue properties (EMTP)-study group's recommended QSM resolution of 1 mm isotropic for

clinical applications<sup>39</sup>. Identifying similar correlations of  $\chi$ <sup>13</sup> (and more, PCS/DCS) in the whole (un-parcellated) substantia nigra with DaT-SPECT at this resolution suggests easier clinical transferability.

Alongside correlations between DaT-SPECT SBR Z-scores and substantia nigra  $\chi$  and PCS, we identified significant negative correlations between SBR Z-scores and DCS at the putamen level in prodromal aSyn patients. A decrease in DCS is indicative of a loss of diamagnetic sources, such as myelin, thereby increasing the average  $\chi$ . [<sup>123</sup>I]FP-CIT uptake in the putamen is linked with nigral neuronal density<sup>65</sup> indicating that dopaminergic cell loss in the substantia nigra is linked to greater dopaminergic projections loss in the striatum. At clinical presentation of overt PD, between 40–60% of dopaminergic neurons are already degenerated in the substantia nigra<sup>66,67</sup> with up to 80% of the axonal terminals in the striatum being lost, particularly in the putamen<sup>67–69</sup>. Axonal loss of dopaminergic neurons in the striatum has been shown to occur in the prodromal phases of alpha-synucleinopathies<sup>67,70–72</sup>. It has been reported that dopaminergic neurons vulnerable to idiopathic PD, are those with long, thin and poorly myelinated axons, whereas those neurons with thicker and more heavily myelinated axons are more resistant to pathology<sup>73–77</sup>. Therefore, we could associate the reduction in the concentration of diamagnetic sources with the loss of thinly myelinated axon terminals in the putamen from degenerated nigrostriatal neurons. Although, we would expect the effect of myelin to be small due to the unmyelinated or lightly myelinated axonal terminals. This, however, must be weighed against the substantial loss of axonal terminals that occur in prodromal alpha-synucleinopathies; a loss of many lightly myelinated axons may still be detectable by measuring the DCS. Further radiological/pathological validation is required.

The lack of correlations of MDS-UPDRS III and MMSE scores, measures of motor disability and mild cognitive impairment, respectively, with DaT-SPECT,  $\chi$ , PCS and DCS are not surprising given the investigation took place in the prodromal cohort, with patients that have not become symptomatic of overt alpha-synucleinopathies yet. Prodromal negative and prodromal positive aSyn patients showed no differences in MDS-UPDRS III or MMSE, which, therefore, would suggest any dopaminergic degeneration measured by DaT-SPECT has not yet manifested itself as motor and cognitive symptoms. These results agree with those of Varga et al.<sup>13</sup> where no correlations were found between bulk  $\chi$  in the whole-brain with MDS-UPDRS III disability scores nor MoCA cognitive scores in both iRBD and Parkinson's disease patients. However, Uchida et al.<sup>14</sup> did identify significant positive correlations between bulk  $\chi$  in the putamen with MDS-UPDRS III and significant negative correlations between bulk  $\chi$  in the caudate with MoCA cognitive scores in Parkinson's disease. While differences in inclusion criteria, the extent and variability of motor/cognitive impairment and medical intervention could represent the key factors underlying the observed differences among studies, further investigations in larger cohorts including both early and advanced prodromal stages are required to better understand these associations.

Limitations include relatively small sample sizes for the DaT-SPECT separated prodromal aSyn groups. Larger sample sizes would strengthen the statistical findings. Additionally, the prodromal and overt aSyn groups included different diagnoses (iRBD/pDLB for prodromal and PD/DLB for overt). With larger samples, these could be included as confounding covariates in a more complex model to better understand subtle differences between aSyn phenotypes. DaT-SPECT SBR Z-scores were only available for the prodromal group; future work should include DaT-SPECT data from both prodromal and overt stages to propose  $\chi$ , PCS and DCS as biomarkers for substantia nigra neurodegeneration across the alpha-synucleinopathy continuum.

Strengths include the novel MRI approach, allowing more specific investigations into paramagnetic and diamagnetic changes compared to standard QSM; the use of DECOMPOSE in a clinically standardized MRI acquisition<sup>33,39</sup>; and the availability of both MRI-QSM and DaT-SPECT data in the same prodromal group, enabling head-to-head comparison of these techniques, minimally explored in the literature, especially in prodromal alpha-synucleinopathies<sup>13,15,25</sup>.

In conclusion, bulk magnetic susceptibility,  $\chi$ , and its paramagnetic component, PCS, can detect iron accumulation in the substantia nigra during the prodromal stages of alpha-synucleinopathies prior to phenoconversion to overt stages. Higher  $\chi$  and PCS, indicating greater iron accumulation, and lower [DCS], indicating possible axonal loss in the nigrostriatal terminals of the putamen, correlate with greater dopaminergic degeneration in the putamen as assessed by DaT-SPECT. Magnetic susceptibility and its paramagnetic and diamagnetic components calculated from DECOMPOSE may serve as non-invasive biomarkers for assessing substantia nigra neurodegeneration and dopaminergic function from prodromal to overt alpha-synucleinopathy stages.

## Data availability

The data that supports the findings of this manuscript are available upon request from the corresponding author, after clearance from the IRB.

Received: 20 September 2024; Accepted: 16 December 2024

Published online: 04 February 2025

## References

- Brás, I. C. & Outeiro, T. F. Alpha-synuclein: Mechanisms of release and pathology progression in synucleinopathies, doi: <https://doi.org/10.3390/cells10020375> (2021).
- Tinaz, S. et al. Semiquantitative analysis of dopamine transporter scans in patients with parkinson disease. *Clinical nuclear medicine* **43**, e1. <https://doi.org/10.1097/RLU.0000000000001885> (2018).
- Simuni, T. et al. A biological definition of neuronal alpha-synuclein disease: towards an integrated staging system for research[SPACE][https://doi.org/10.1016/S1474-4422\(23\)00405-2](https://doi.org/10.1016/S1474-4422(23)00405-2) (2024).
- Seibyl, J. P. & Kuo, P. What is the role of dopamine transporter imaging in parkinson prevention clinical trials?. *Neurology* **99**, S61–S67. <https://doi.org/10.1212/WNL.000000000000200786> (2022).
- Postuma, R. B. et al. Risk and predictors of dementia and parkinsonism in idiopathic rem sleep behaviour disorder: a multicentre study. *Brain* **142**, 744–759. <https://doi.org/10.1093/brain/awz030> (2019).

6. McKeith, I. G. et al. Research criteria for the diagnosis of prodromal dementia with lewy bodies. *Neurology* **94**, 743–755. [https://doi.org/10.1212/WNL.0000000000009323/ASSET/9D505976-0B14-4F1B-8306-0A8334F14282/ASSETS/GRAPHIC/16TTU1BJP EG](https://doi.org/10.1212/WNL.0000000000009323/ASSET/9D505976-0B14-4F1B-8306-0A8334F14282/ASSETS/GRAPHIC/16TTU1BJP EG (2020).) (2020).
7. Arnaldi, D. et al. Dopaminergic imaging and clinical predictors for phenoconversion of rem sleep behaviour disorder. *Brain* **144**, 278–287. <https://doi.org/10.1093/brain/awaa365> (2021).
8. Arnaldi, D. et al. Presynaptic dopaminergic imaging characterizes patients with rem sleep behavior disorder due to synucleinopathy. *Annals of Neurology* **95**, 1178–1192. <https://doi.org/10.1002/ANA.26902> (2024).
9. Lanfranchi, F. et al. Different z-score cut-offs for striatal binding ratio (sbr) of dat spect are needed to support the diagnosis of parkinson's disease (pd) and dementia with lewy bodies (dlb). *European Journal of Nuclear Medicine and Molecular Imaging* **50**, 1090–1102. <https://doi.org/10.1007/s00259-022-06069-0> (2023).
10. Höglinger, G. U. et al. A biological classification of parkinson's disease: the synneurge research diagnostic criteria. *The Lancet Neurology* **23**, 191–204. [https://doi.org/10.1016/S1474-4422\(23\)00404-0](https://doi.org/10.1016/S1474-4422(23)00404-0) (2024).
11. Barber, T. R. et al. Nigrosome 1 imaging in rem sleep behavior disorder and its association with dopaminergic decline. *Annals of Clinical and Translational Neurology* **7**, 26–35. <https://doi.org/10.1002/acn3.50962> (2020).
12. Lancione, M. et al. Evaluation of iron overload in nigrosome 1 via quantitative susceptibility mapping as a progression biomarker in prodromal stages of synucleinopathies. *NeuroImage* **260**, 119454. <https://doi.org/10.1016/J.NEUROIMAGE.2022.119454> (2022).
13. Varga, Z. et al. Whole brain pattern of iron accumulation in rem sleep behavior disorder. *Human Brain Mapping* **45**, doi: <https://doi.org/10.1002/hbm.26675> (2024).
14. Uchida, Y. et al. Magnetic susceptibility associates with dopaminergic deficits and cognition in parkinson's disease. *Movement Disorders* **35**, 1396–1405. <https://doi.org/10.1002/mds.28077> (2020).
15. Frosini, D. et al. Seven tesla mri of the substantia nigra in patients with rapid eye movement sleep behavior disorder. *Parkinsonism & Related Disorders* **43**, 105–109. <https://doi.org/10.1016/J.PARKRELDIS.2017.08.002> (2017).
16. Shmueli, K. Chapter 31 - quantitative susceptibility mapping. In Seiberlich, N. et al. (eds.) *Quantitative Magnetic Resonance Imaging*, vol. 1 of *Advances in Magnetic Resonance Technology and Applications*, 819–838, doi: <https://doi.org/10.1016/B978-0-12-817057-1.00033-0> (Academic Press, 2020).
17. Shmueli, K. et al. Magnetic susceptibility mapping of brain tissue in vivo using mri phase data. *Magnetic Resonance in Medicine* **62**, 1510–1522. <https://doi.org/10.1002/mrm.22135> (2009).
18. Reichenbach, J. R., Schweser, F., Serres, B. & Deistung, A. Quantitative susceptibility mapping: Concepts and applications. *Clinical Neuroradiology* **25**, 225–230. <https://doi.org/10.1007/s00062-015-0432-9> (2015).
19. Deistung, A., Schweser, F. & Reichenbach, J. R. Overview of quantitative susceptibility mapping. *NMR in Biomedicine* **30**, doi: <https://doi.org/10.1002/nbm.3569> (2017).
20. Rochefort, L. D., Brown, R., Prince, M. R. & Wang, Y. Quantitative mr susceptibility mapping using piece-wise constant regularized inversion of the magnetic field. *Magnetic Resonance in Medicine* **60**, 1003–1009. <https://doi.org/10.1002/mrm.21710> (2008).
21. An, H. et al. Quantifying iron deposition within the substantia nigra of parkinson's disease by quantitative susceptibility mapping. *Journal of the Neurological Sciences* **386**, 46–52. <https://doi.org/10.1016/j.jns.2018.01.008> (2018).
22. Mazzucchi, S. et al. Quantitative susceptibility mapping in atypical parkinsonisms. *NeuroImage: Clinical* **24**, doi: <https://doi.org/10.1016/j.nicl.2019.101999> (2019).
23. Langkammer, C. et al. Quantitative susceptibility mapping in parkinson's disease. *PLoS ONE* **11**, 1–13. <https://doi.org/10.1371/journal.pone.0162460> (2016).
24. Thomas, G. E. C. et al. Brain iron deposition is linked with cognitive severity in parkinson's disease. *Journal of Neurology, Neurosurgery and Psychiatry* 418–425, doi: <https://doi.org/10.1136/jnnp-2019-322042> (2020).
25. Biondetti, E. et al. The spatiotemporal changes in dopamine, neuromelanin and iron characterizing parkinson's disease. *Brain* **144**, 3114–3125. <https://doi.org/10.1093/BRAIN/AWAB191> (2021).
26. Chen, J., Gong, N. J., Chaim, K. T., Otaduy, M. C. G. & Liu, C. Decompose quantitative susceptibility mapping (qsm) to sub-voxel diamagnetic and paramagnetic components based on gradient-echo mri data. *NeuroImage* **242**, doi: <https://doi.org/10.1016/j.neuroimage.2021.118477> (2021).
27. Ahmed, M. et al. The diamagnetic component map from quantitative susceptibility mapping (qsm) source separation reveals pathological alteration in alzheimer's disease-driven neurodegeneration. *NeuroImage* **280**, doi: <https://doi.org/10.1016/j.neuroimage.2023.120357> (2023).
28. Fushimi, Y. et al. Value of quantitative susceptibility mapping in clinical neuroradiology. *Journal of Magnetic Resonance Imaging* **59**, 1914–1929. <https://doi.org/10.1002/JMRI.29010> (2024).
29. van Steenoven, I. et al. Conversion between mini-mental state examination, montreal cognitive assessment, and dementia rating scale-2 scores in parkinson's disease. *Movement Disorders* **29**, 1809–1815 (2014).
30. Postuma, R. B. et al. Mds clinical diagnostic criteria for parkinson's disease. *Movement Disorders* **30**, 1591–1601. <https://doi.org/10.1002/MDS.26424> (2015).
31. Thorpy, M. *International Classification of Sleep Disorders* (American Academy of Sleep Medicine, 2014), 3 edn.
32. McKeith, I. G. et al. Diagnosis and management of dementia with lewy bodies. *Neurology* **89**, 88–100. [https://doi.org/10.1212/WNL.0000000000004058/SUPPL\\_FILE/18.PDF](https://doi.org/10.1212/WNL.0000000000004058/SUPPL_FILE/18.PDF) (2017).
33. Lancione, M. et al. Multi-centre and multi-vendor reproducibility of a standardized protocol for quantitative susceptibility mapping of the human brain at 3t. *Physica Medica* **103**, 37–45. <https://doi.org/10.1016/j.ejmp.2022.09.012> (2022).
34. Kiersnowski, O. C., Karsa, A., Wastling, S. J., Thornton, J. S. & Shmueli, K. Investigating the effect of oblique image acquisition on the accuracy of qsm and a robust tilt correction method. *Magnetic Resonance in Medicine* [SPACE] <https://doi.org/10.1002/mrm.29550> (2022).
35. Jenkinson, M. & Smith, S. A global optimisation method for robust affine registration of brain images. *Medical Image Analysis* **5**, 143–156. [https://doi.org/10.1016/S1361-8415\(01\)00036-6](https://doi.org/10.1016/S1361-8415(01)00036-6) (2001).
36. Jenkinson, M., Bannister, P., Brady, M. & Smith, S. Improved optimization for the robust and accurate linear registration and motion correction of brain images. *NeuroImage* **17**, 825–841. <https://doi.org/10.1006/NIMG.2002.1132> (2002).
37. Pei, M. et al. Algorithm for fast monoexponential fitting based on auto-regression on linear operations (arlo) of data. *Magnetic Resonance in Medicine* **73**, 843–850. <https://doi.org/10.1002/mrm.25137> (2015).
38. Lab, C. M. R. Medi toolbox.
39. Bilgic, B. et al. Recommended implementation of quantitative susceptibility mapping for clinical research in the brain: A consensus of the ismrm electro-magnetic tissue properties study group. *Magnetic Resonance in Medicine* **91**, 1834–1862. <https://doi.org/10.1002/MRM.30006> (2024).
40. Smith, S. M. Fast robust automated brain extraction. *Human Brain Mapping* **17**, 143–155. <https://doi.org/10.1002/hbm.10062> (2002).
41. Liu, T. et al. Nonlinear formulation of the magnetic field to source relationship for robust quantitative susceptibility mapping. *Magnetic Resonance in Medicine* **69**, 467–476. <https://doi.org/10.1002/mrm.24272> (2013).
42. Schofield, M. A. & Zhu, Y. Fast phase unwrapping algorithm for interferometric applications. *Optics Letters* **28**, 1194. <https://doi.org/10.1364/ol.28.001194> (2003).

43. Schweser, F., Deistung, A., Lehr, B. W. & Reichenbach, J. R. Quantitative imaging of intrinsic magnetic tissue properties using mri signal phase: An approach to in vivo brain iron metabolism?. *NeuroImage* **54**, 2789–2807. <https://doi.org/10.1016/j.neuroimage.2010.10.070> (2011).
44. Li, W. et al. A method for estimating and removing streaking artifacts in quantitative susceptibility mapping. *NeuroImage* **108**, 111–122. <https://doi.org/10.1016/j.neuroimage.2014.12.043> (2015).
45. Li, X. et al. Multi-atlas tool for automated segmentation of brain gray matter nuclei and quantification of their magnetic susceptibility. *NeuroImage* **191**, 337–349. <https://doi.org/10.1016/j.neuroimage.2019.02.016> (2019).
46. Mori, S. et al. Mricloud: Delivering high-throughput mri neuroinformatics as cloud-based software as a service. *Computing in Science and Engineering* **18**, 21–35. <https://doi.org/10.1109/MCSE.2016.93> (2016).
47. Darcourt, J. et al. Eanm procedure guidelines for brain neurotransmission spect using 123i-labelled dopamine transporter ligands, version 2. *European Journal of Nuclear Medicine and Molecular Imaging* **37**, 443–450. <https://doi.org/10.1007/S00259-009-1267-X/TABLES/2> (2010).
48. Maltais, D. D. et al. Confirmation of 123i-fp-cit spect quantification methods in dementia with lewy bodies and other neurodegenerative disorders. *Journal of Nuclear Medicine* **61**, 1628–1635. <https://doi.org/10.2967/JNUMED.119.239418> (2020).
49. Chen, Q. et al. beta-amyloid pet and 123i-fp-cit spect in mild cognitive impairment at risk for lewy body dementia. *Neurology* **96**, E1180–E1189. <https://doi.org/10.1212/WNL.00000000000011454/ASSET/1C9CC2C2-E343-492F-AD01-0BAFE214A37E/ASSET/S/GRAPHIC/12TTU1.GIF> (2021).
50. Li, W. et al. Differential developmental trajectories of magnetic susceptibility in human brain gray and white matter over the lifespan. *Human Brain Mapping* **35**, 2698–2713. <https://doi.org/10.1002/hbm.22360> (2014).
51. Zhang, Y. et al. Longitudinal atlas for normative human brain development and aging over the lifespan using quantitative susceptibility mapping. *NeuroImage* **171**, 176–189. <https://doi.org/10.1016/j.neuroimage.2018.01.008> (2018).
52. Kiersnowski, O. C. et al. Quantitative susceptibility mapping identifies hippocampal and other subcortical grey matter tissue composition changes in temporal lobe epilepsy. *Human Brain Mapping* **44**, 5047–5064. <https://doi.org/10.1002/HBM.26432> (2023).
53. Duyn, J. H. & Schenck, J. *Contributions to magnetic susceptibility of brain tissue*[SPACE]<https://doi.org/10.1002/nbm.3546> (2017).
54. Li, W., Jiang, H., Song, N. & Xie, J. Oxidative stress partially contributes to iron-induced alpha-synuclein aggregation in sk-n-sh cells. *Neurotoxicity Research* **19**, 435–442. <https://doi.org/10.1007/S12640-010-9187-X/FIGURES/5> (2011).
55. Shin, H. G. et al.  $\chi$ -separation: Magnetic susceptibility source separation toward iron and myelin mapping in the brain. *NeuroImage* **240**, 118371. <https://doi.org/10.1016/j.neuroimage.2021.118371> (2021).
56. Li, Z. et al. Apart-qsm: An improved sub-voxel quantitative susceptibility mapping for susceptibility source separation using an iterative data fitting method. *NeuroImage* **274**, 120148. <https://doi.org/10.1016/j.neuroimage.2023.120148> (2023).
57. Madden, D. J. & Merenstein, J. L. Quantitative susceptibility mapping of brain iron in healthy aging and cognition. *NeuroImage* **282**, 120401. <https://doi.org/10.1016/j.neuroimage.2023.120401> (2023).
58. Murakami, Y. et al. Usefulness of quantitative susceptibility mapping for the diagnosis of parkinson disease. *American Journal of Neuroradiology* **36**, 1102–1108. <https://doi.org/10.3174/ajnr.A4260> (2015).
59. Barbosa, J. H. O. et al. Quantifying brain iron deposition in patients with parkinson's disease using quantitative susceptibility mapping, r2 and r2\*. *Magnetic Resonance Imaging* **33**, 559–565. <https://doi.org/10.1016/j.mri.2015.02.021> (2015).
60. Yu, K. et al. Direct visualization of deep brain stimulation targets in patients with parkinson's disease via 3-t quantitative susceptibility mapping. *Acta Neurochirurgica*[SPACE]<https://doi.org/10.1007/s00701-021-04715-4/Published> (2021).
61. Li, K. et al. Quantification of brain iron accumulation in different stages of parkinson's disease using quantitative susceptibility mapping (qsm) (2181). *Neurology* **96**, 2181. [https://doi.org/10.1212/WNL.96.15\\_supplement.2181](https://doi.org/10.1212/WNL.96.15_supplement.2181) (2021).
62. Huang, W. et al. Quantitative susceptibility mapping versus phase imaging to identify multiple sclerosis iron rim lesions with demyelination. *Journal of Neuroimaging* **32**, 667–675. <https://doi.org/10.1111/JON.12987> (2022).
63. Kuya, K. et al. Evaluation of parkinson's disease by neuromelanin-sensitive magnetic resonance imaging and 123i-fp-cit spect. <https://doi.org/10.1177/0284185117722812> **59**, 593–598, doi: <https://doi.org/10.1177/0284185117722812>(2017).
64. Zeng, W., Cai, J., Zhang, L. & Peng, Q. Iron deposition in parkinson's disease: A mini-review. *Cellular and Molecular Neurobiology* **2024** 44:1 **44**, 1–12, doi: <https://doi.org/10.1007/S10571-024-01459-4>(2024).
65. Colloby, S. J., McParland, S., O'Brien, J. T. & Attems, J. Neuropathological correlates of dopaminergic imaging in alzheimer's disease and lewy body dementias. *Brain* **135**, 2798–2808. <https://doi.org/10.1093/BRAIN/AWS211> (2012).
66. Madeo, G. et al. On cell loss and selective vulnerability of neuronal populations in parkinson's disease. *Frontiers in Neurology* | [www.frontiersin.org](http://www.frontiersin.org) **1**, 455, doi: <https://doi.org/10.3389/fneur.2018.00455>(2018).
67. Gcwensa, N. Z., Russell, D. L., Cowell, R. M. & Volpicelli-Daley, L. A. Molecular mechanisms underlying synaptic and axon degeneration in parkinson's disease. *Frontiers in Cellular Neuroscience* **15**, doi: <https://doi.org/10.3389/FNCEL.2021.626128>(2021).
68. Kurowska, Z. et al. Is axonal degeneration a key early event in parkinson's disease?. *Journal of Parkinson's Disease* **6**, 703–707. <https://doi.org/10.3233/JPD-160881> (2016).
69. Kordower, J. H. et al. Disease duration and the integrity of the nigrostriatal system in parkinson's disease. *Brain* **136**, 2419. <https://doi.org/10.1093/BRAIN/AWT192> (2013).
70. Delva, A., Weehaeghe, D. V., Koole, M., Laere, K. V. & Vandenbergh, W. Loss of presynaptic terminal integrity in the substantia nigra in early parkinson's disease. *Movement Disorders* **35**, 1977–1986. <https://doi.org/10.1002/MDS.28216> (2020).
71. Fazio, P. et al. Nigrostriatal dopamine transporter availability in early parkinson's disease. *Movement Disorders* **33**, 592–599. <https://doi.org/10.1002/MDS.27316> (2018).
72. Jennings, D. et al. Conversion to parkinson disease in the pars hypophysialis and dopamine transporter-deficit prodromal cohort. *JAMA Neurology* **74**, 933–940. <https://doi.org/10.1001/JAMANEUROL.2017.0985> (2017).
73. Braak, H. & Tredici, K. D. Poor and protracted myelination as a contributory factor to neurodegenerative disorders. *Neurobiology of Aging* **25**, 19–23. <https://doi.org/10.1016/j.neurobiolaging.2003.04.001> (2004).
74. Braak, H., Rüb, U., Gai, W. P. & Tredici, K. D. Idiopathic parkinson's disease: possible routes by which vulnerable neuronal types may be subject to neuroinvasion by an unknown pathogen. *J Neural Transm* **110**, 517–536. <https://doi.org/10.1007/s00702-002-0808-2> (2003).
75. Braak, H. et al. Staging of brain pathology related to sporadic parkinson's disease. *Neurobiology of Aging* **24**, 197–211. [https://doi.org/10.1016/S0197-4580\(02\)00065-9](https://doi.org/10.1016/S0197-4580(02)00065-9) (2003).
76. Braak, H., Vos, R. A. D., Jansen, E. N., Bratzke, H. & Braak, E. Chapter 20 neuropathological hallmarks of alzheimer's and parkinson's diseases. *Progress in Brain Research* **117**, 267–285, doi: [https://doi.org/10.1016/S0079-6123\(08\)64021-2](https://doi.org/10.1016/S0079-6123(08)64021-2)(1998).
77. Wong, Y. C. et al. Neuronal vulnerability in parkinson disease: Should the focus be on axons and synaptic terminals?. *Movement Disorders* **34**, 1406–1422. <https://doi.org/10.1002/MDS.27823> (2019).

## Acknowledgements

The authors would like to thank all the participants for their time, Dr Patrick Fuchs for advice in implementing DECOMPOSE, and Prof Alessio Signori for helpful discussions about the statistical analysis.

## Author contributions

O.C.K. contributed to the conception of the work, data processing, statistical analysis, interpretation of results and drafted the main body of the manuscript. L.Ar., L.Av., E.P., M.L. and B.O. contributed to data acquisition. F.C., L.F. and P.M. contributed to data acquisition, processing and interpretation of results. A.D. contributed to data analysis and interpretation of results. C.L. and F.M. contributed to data processing and interpretation of results. S.M. and S.R. contributed to data acquisition and data processing. M.C. contributed to the conception of the work, data processing, interpretation of results and drafting the manuscript. M.P., D.A. and L.R. contributed to the conception of the work, interpretation of results and drafting the manuscript. All authors reviewed, edited and approved the final version of the manuscript.

## Funding

This work was supported by: #NEXTGENERATIONEU (NGEU), funded by the Ministry of University and Research (MUR), National Recovery and Resilience Plan (NRRP), project RAISE (ECS00000035) Robotics and AI for Socio-economic Empowerment (DN. 1053 23.06.2022), for the activities of Luca Roccatagliata. #NEXTGENERATIONEU (NGEU), funded by the Ministry of University and Research (MUR), National Recovery and Resilience Plan (NRRP), project MNESYS (PE0000006) A Multiscale integrated approach to the study of the nervous system in health and disease (DN. 1553 11.10.2022) for the activities of Laura Avanzino, Andrea Diociasi, Federico Massa and Elisa Pelosin. #NEXTGENERATIONEU (NGEU), funded by the European Union, NRRP M6C2 – Investment 2.1 Enhancement and strengthening of biomedical research in the NHS (PN-RR-MCNT2-2023-12377527 - CUP C13C23001070006) for the activities of Matteo Pardini. 5×mille, funded by the Italian Ministry of Health, for the activities of Oliver C. Kiersnowski. FRA2022/DINOGMI – Department of Neuroscience, Rehabilitation, Ophthalmology, Genetics, Maternal and Child Health, funded by the Italian Ministry of University and Research (MUR), for the activities of Mauro Costagli.

## Declarations

### Competing interests

The authors declare no competing interests. FM received speaker honoraria from Roche Diagnostics S.p.A and Eli Lilly S.p.A.

### Additional information

**Correspondence** and requests for materials should be addressed to L.R.

**Reprints and permissions information** is available at [www.nature.com/reprints](http://www.nature.com/reprints).

**Publisher's note** Springer Nature remains neutral with regard to jurisdictional claims in published maps and institutional affiliations.

**Open Access** This article is licensed under a Creative Commons Attribution-NonCommercial-NoDerivatives 4.0 International License, which permits any non-commercial use, sharing, distribution and reproduction in any medium or format, as long as you give appropriate credit to the original author(s) and the source, provide a link to the Creative Commons licence, and indicate if you modified the licensed material. You do not have permission under this licence to share adapted material derived from this article or parts of it. The images or other third party material in this article are included in the article's Creative Commons licence, unless indicated otherwise in a credit line to the material. If material is not included in the article's Creative Commons licence and your intended use is not permitted by statutory regulation or exceeds the permitted use, you will need to obtain permission directly from the copyright holder. To view a copy of this licence, visit <http://creativecommons.org/licenses/by-nc-nd/4.0/>.

© The Author(s) 2025